LARGE EDDY SIMULATION OF FREE SURFACE FLOW

Hua Ji*
Department of Mechanical Engineering,
University of Waterloo
Waterloo, Ontario N2L 3G1, Canada
huaji2005@gmail.com

Fue-Sang Lien
Department of Mechanical Engineering,
University of Waterloo
Waterloo, Ontario N2L 3G1, Canada
fslien@sunwise.uwaterloo.ca

Al B. Strong
Department of Mechanical Engineering,
University of Waterloo
Waterloo, Ontario N2L 3G1, Canada
astrong@sunwise.uwaterloo.ca

ABSTRACT

A front tracking method is developed for three dimensional free surface problems. Triangulated surface meshes are used to represent the free surface and compute the geometric parameters. The volume fraction of fluid and the surface area cut by the interface in a Cartesian control volume are computed in terms of boolean operations. The normal stress boundary conditions are added at the exact location of the interface. The tangential stress boundary conditions are enhanced with the least squares technique when the velocity boundary conditions are extrapolated. The Cartesian grid method (or cut-cell method) is used to discretize the governing equations and treat the interface as a sharp discontinuity. This method is applied to implement LES of free surface flows in an open channel with small amplitude waves. The numerical results are in excellent agreement with experimental and DNS data.

INTRODUCTION

Turbulence phenomena on the surfaces of rivers, lakes and seas have been observed and reported for centuries. Examples include surges on the sea and waves on steep rivers. From an engineering point of view, an understanding of the dynamics of free surface turbulence in an open channel flow is of great importance because it governs the mechanism of the transfer of mass, heat and momentum across a gas-liquid interface.

Although free surface turbulence has fascinated and attracted many researchers, it has also presented a great challenge to them. Until recently, very limited knowledge about the structure of turbulence near the free surface has been obtained either experimentally or numerically. This can be attributed to two main reasons: firstly, it is very difficult to make measurements of velocity and turbulence near a moving free surface, and secondly, from a numerical point of view, the complex moving boundary makes simulations very difficult to perform with high precision. In spite of this, a great deal of effort has been undertaken over the last two decades to develop an understanding of free surface turbulence (Nezu (1993), Komori (1982), Kumar (1998)).

A review of these references reveals some important findings about the nature of near free surface turbulence's coherent structures and it is worthwhile to mention these here: (1) near the free surface the turbulent kinetic energy of vertical velocity fluctuations is redistributed to horizontal motions, (2) the surface normal vortices deform the free surface, (3) large eddies with axes nearly parallel to the free surface are flattened by the free surface, (4) flow structures can be classified as upwellings, downdrafts, or spiral eddies.

Numerical computations mostly assume a rigid slip surface and ignore the vertical motion of the free surface (Pan (1995)). This reduces the complexity of the algorithm used to compute the surface at the cost of losing the physics of the free surface interaction with respect to energy transfer. Some researchers (Komori (1982), Nakayama (2002)) use the body-fitted method to obtain a DNS computation of the free surface for which the solutions are restricted to situations of small amplitude deformation. Very recently, Nakayama et al. (2002) performed a very fine grid DNS (2 million points) for free surface flows with small amplitude deformation.

The proposed front tracking method is applied here to perform large eddy simulation of the free surface flow with small amplitude surface deformation. With the comparison of the fine resolution DNS results by Nakayama et al. (2002) and experimental results by Kumar et al. (1998), it is demonstrated that this front tracking method can be used to successfully simulate this complex turbulent flow.

*Current address: Waterloo CFD Engineering Consulting Inc.

MATHEMATICAL FORMULATION

The Cartesian tensor equations of motion for the spatially filtered incompressible velocity and pressure fields are given by

$$\frac{\partial \overline{u}_i}{\partial x_i} = 0, \tag{1}$$

$$\frac{\partial \overline{u}_i}{\partial t} + \frac{\partial \overline{u}_i \overline{u}_j}{\partial x_j} = -\frac{\partial \overline{p}}{\partial x_i} + \frac{\partial}{\partial x_j}\left((\nu + \nu_t)\left(\frac{\partial \overline{u}_j}{\partial x_i} + \frac{\partial \overline{u}_i}{\partial x_j}\right)\right) + \overline{g}_i, \tag{2}$$

where the overbar represents the spatial filtering on the scale of the grid. The gravitational acceleration $\overline{g}_i$ is kept in equation (2) since the free surface is allowed to move freely. Equation (2) assumes Boussinesq dynamics to approximate the subgrid stresses, where the subgrid viscosity, ν_t, is given by the Smagorinsky closure

$$\nu_t = C\overline{\Delta}^2\sqrt{2\overline{S}_{ij}\overline{S}_{ij}}. \tag{3}$$

In equation (3), the resolved strain rate tensor is defined as

$$\overline{S}_{ij} = \frac{1}{2}\left(\frac{\partial \overline{u}_j}{\partial x_i} + \frac{\partial \overline{u}_i}{\partial x_j}\right). \tag{4}$$

The Smagorinsky "constant", C, is calculated locally using the dynamic procedure of Lilly (1992) with averaging in the homogeneous directions to avoid the numerical instability associated with large negative C values.

NUMERICAL METHOD

Tracking the interface

A surface mesh is used to define the interface. The surface mesh is composed of many connected triangular elements with the marker points as their vertices, as shown in Fig. 1. If one views a triangle from outside of the fluid, its edges are considered in a counter-clockwise direction so that the normal direction of the interface points outside of the fluid (see Fig. 1, in which n_i is the normal direction of the triangle i).

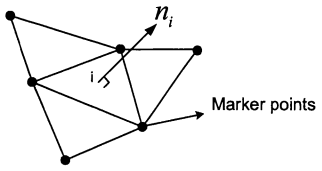

Figure 1: Three dimensional structure of the interface

Computing the geometric parameters

Boolean operations between Cartesian meshes and the interface are used to compute these parameters. This is a difficult problem to solve in a robust manner (due to the limited precision of arithmetic operations in computers). An approach similar to that presented by Aftosmis et al. (1997), which was successfully used to handle three dimensional complex solid geometry problems with the Cartesian grid method, is used to implement the current Boolean operations. The computation of the volume and the surface area fraction in a Cartesian cell is divided into four steps:

Step 1: For each Cartesian cell, check if any of the 12 triangles is cut by the interface which has already been triangulated. If yes, compute the pierce points, and connect the two pierce points on the triangle as a cut edge. The cut edges are stored in a new linked list. The signed volume of the tetrahedron T_{abcd} in determinant form (5) is used to check if any two triangles are cut by each other.

$$6V(T_{abcd}) = \det\begin{pmatrix} a_x - d_x & a_y - d_y & a_z - d_z \\ b_x - d_x & b_y - d_y & b_z - d_z \\ c_x - d_x & c_y - d_y & c_z - d_z \end{pmatrix}, \tag{5}$$

where a, b and c are three vertices of a triangle, and d is one of the vertices of another triangle.This will be the case only if the three tetrahedra formed by connecting the end points of edge de with two of the three vertices of the triangle have the same sign (Aftosmis et al. (1997)), that is:

$$\begin{aligned} V(T_{dabe}) &> 0 \text{ and } V(T_{dbce}) > 0 \text{ and } V(T_{dcae}) > 0, \text{ or} \\ V(T_{dabe}) &< 0 \text{ and } V(T_{dbce}) < 0 \text{ and } V(T_{dcae}) < 0. \end{aligned} \tag{6}$$

Fig. 2 illustrates this test for the case that the three volumes are all positive.

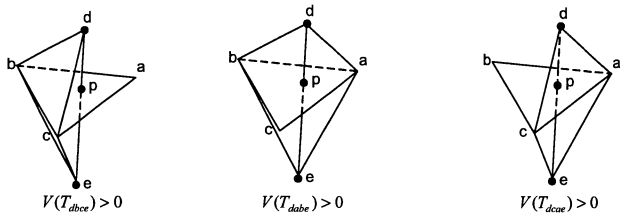

Figure 2: Boolean test for the pierce of a line segment de within across the boundary of a triangle Δ_{abc}

As we know, a zero-volume tetrahedron represents the case that the four vertices are co-planar. However, obtaining the zero-volume value is difficult, since it requires that we distinguish round-off error from exactly zero. The adaptive precision exact arithmetic procedure developed by Schewchuk (1996) is used to implement the computation. If this result is identically zero, we then resolve the degeneracy with a general tie-breaking algorithm based on a virtual perturbation approach (Edelsbrunner (1990)).

Step 2: Fig. 3 shows a triangle with three intersections. The segments divide the intersected triangle into polygonal regions (polygon P_{ab4321} and P_{1234c} in the Fig. 3) which are either completely inside or outside of the body. In order to determine the inside or outside parts, we triangulate these polygonal regions within each intersected triangle.

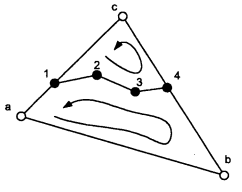

Figure 3: A triangle with three intersections

Step 3: The ray-casting approach (Aftosmis et al. (1997)) is used to determine if the point is inside or outside part of

a surface relative to another surface in order to compute the volume or area fraction of the fluid. As indicated in Fig. 4, one casts a ray r from p and simply counts the number of intersections of r. If the point lies outside of polygon m, the number is even, and if the point is contained, this result is odd.

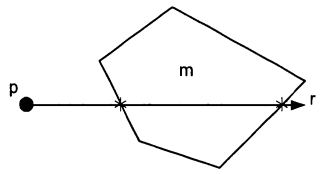

Figure 4: Illustration of point-in-polygon with the ray-casting approach

Step 4: After the boolean operations, the closed triangulated surface will be obtained. Based on the Gauss Theorem, the volume integral can be transformed to a corresponding surface integral. The sum of the surface integrals for each of these triangles is the volume fraction of fluid. The area fraction cut by the interface can be computed by adding each triangle's area.

Implementation of free surface boundary conditions

The normal and tangential stress boundary conditions on the free surface can be written as

$$p = p_0 + \sigma\kappa + \mu n_i \left(\frac{\partial u_i}{\partial x_j} + \frac{\partial u_j}{\partial x_i}\right) n_j, \tag{7}$$

for the pressure, and for the stresses,

$$t_i \left(\frac{\partial u_i}{\partial x_j} + \frac{\partial u_j}{\partial x_i}\right) n_j = 0, \tag{8}$$

where p_0 is the pressure in the air, σ is the surface tension coefficient, n_i is the unit vector normal to the interface, t_i is the vector tangent to the interface, μ is the dynamic viscosity.

In order to get the boundary velocity value, it is assumed that the boundary velocity field varies linearly, i.e.

$$u = a_u + b_u x + c_u y,\ v = a_v + b_v x + c_v y,\ w = a_w + b_w x + c_w y. \tag{9}$$

For free surface problems, the velocity fields around the interface also have to satisfy equation (8). To enforce this condition, we use the least squares technique to determine the unknown parameters in equation (9) with the constraint of the tangential stress boundary condition. Thus, we obtain the expression:

$$\begin{aligned}\Phi \;=\; & \sum_{m=1}^{N} [a_u + b_u(x_u)_m + c_u(y_u)_m + d_u(z_u)_m - u_m]^2 \\ & + \sum_{m=1}^{N} [a_v + b_v(x_v)_m + c_v(y_v)_m + d_v(z_v)_m - v_m]^2 \\ & + \sum_{m=1}^{N} [a_w + b_w(x_w)_m + c_w(y_w)_m + d_w(z_w)_m - w_m]^2 \\ & + \lambda_1 t_i D_{ij} n_j + \lambda_2 l_i D_{ij} n_j,\end{aligned} \tag{10}$$

where λ_1 and λ_2 are Lagrange multipliers; N is the number of selected points near the interface (five points are usually chosen); $(x_u, y_u, z_u)_m$, $(x_v, y_v, z_v)_m$ and $(x_w, y_w, z_w)_m$ are the position coordinates for the u_m, v_m and w_m velocity components, respectively; t_i and l_i are two orthogonal tangential vectors. With the least squares technique, we can use the 14 linear equations to determine 14 unknowns, which are in the form:

$$C_i = (a_u, b_u, c_u, d_u, a_v, b_v, c_v, d_v, a_w, b_w, c_w, d_w, \lambda_1, \lambda_2). \tag{11}$$

Numerical discretization with cut-cell method

The u momentum equation is used to exemplify the numerical discretization with the cut-cell method. Fig. 5 shows a three dimensional u momentum control volume cut by the interface. The center of the cubic finite domain is at (x_i, y_j, z_k). The boundary velocity (u_g, v_g, w_g) is 0 on $P_{ABFE} \cup P_{BCIHF} \cup P_{DCIJG} \cup P_{ADGE} \cup P_{ABCD} \cup P_{EFHJG}$ and (u, v, w) on the interface HIJ. The u momentum equation can be discretized as

$$\begin{aligned}\frac{\partial}{\partial t}\int_\Omega u dxdydz = & \\ & \int_{P_{BCIHF}}^{P_{ADGE}} p dydz - \int_{HIJ} p n_x ds \\ & + \int_{P_{ADGE}}^{P_{BCIHF}} (S_{xx} - uu)\, dydz + \int_{HIJ} S_{xx} n_x ds \\ & + \int_{P_{ABFE}}^{P_{DCIJG}} (S_{xy} - uv)\, dxdz + \int_{HIJ} S_{yx} n_y ds \\ & + \int_{P_{ABCD}}^{P_{EFHJG}} (S_{xz} - uw)\, dxdy + \int_{HIJ} S_{zx} n_z ds \\ & + \int_\Omega g_x dxdydz.\end{aligned} \tag{12}$$

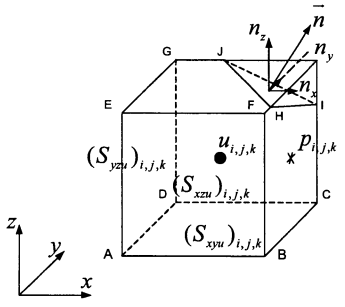

Figure 5: A three dimensional u momentum control volume cut by the interface

Using the symbols shown in Fig 5, the right-hand-side of

equation (12) can be rewritten;

$$
\begin{aligned}
F \;=\; & (S_{yzu})_{i,j,k}p_{i-1,j,k} - (S_{yzu})_{i+1,j,k}p_{i,j,k} \\
& - \int_{HIJ} pn_x ds + [S_{yzu}(S_{xx} - uu)]_{i,j,k}^{i+1,j,k} \\
& + \int_{HIJ} S_{xx}n_x ds + [S_{xzu}\,(S_{yx} - uv)]_{i,j,k}^{i,j+1,k} \\
& + \int_{HIJ} S_{yx}n_y ds + [S_{xyu}\,(S_{zx} - uw)]_{i,j,k}^{i,j,k+1} \\
& + \int_{HIJ} S_{zx}n_z ds + (C_u g_x)_{i,j,k}, \qquad (13)
\end{aligned}
$$

where, e.g., $[S_{yzu}\,(S_{xx} - uu)]_{i,j,k}^{i+1,j,k} = [S_{yzu}\,(S_{xx} - uu)]_{i+1,j,k} - [S_{yzu}\,(S_{xx} - uu)]_{i,j,k}$, and $C_u = \int_\Omega dxdydz$ is the volume fraction of fluid in the control volume.

The same least squares technique is applied to compute the viscous stresses on the centroid of each triangle of the interface. The surface integrals of the normal stress in equation (13) can be evaluated by

$$\int_{HIJ} S_{xx}n_x ds = \sum (S_{xx})_c n_x \Delta s, \qquad (14)$$

where $\int_{HIJ}$ denotes the integration along the piece of the interface contained in the control domain; $(S_{xx})_c$ are the viscous normal stress on the triangle whose area is Δs. Other shear stresses in equation (13) can be expressed similarly to equation (14).

The surface integral of the pressure along the interface involves the integrals of the normal stress and the surface tension (see equation (7)). The integral of the normal stress is computed with the same method as that shown in equation (14). For the computation of the surface tension, we use the same approach as Tryggvason et al. (2001) in their front tracking method:

$$\int_s \sigma\kappa\vec{n}\,ds = \sigma\int_s (\vec{n}\times\nabla)\times\vec{n}\,ds = \sigma\oint_l \vec{t}\times\vec{n}\,dl, \qquad (15)$$

where the Stokes theorem is used to convert the area integral into the line integral along the edges of the triangle.

The normal direction of a triangle is computed directly from the coordinates of the three vertices. The tangent is simply computed by subtracting the end points of the edge. The computation of the normal direction is obtained by averaging the normals $\vec{n_i}$ of the N facets incident into the vertex. The average is weighted by the angle (Thurmer (1998)). As shown in Fig. 6, the normal direction $\vec{n}$ of the vertex $v1$ is computed using

$$\vec{n} = \frac{\sum_{i=1}^{N}\alpha_i\vec{n_i}}{\left|\sum_{i=1}^{N}\alpha_i\vec{n_i}\right|}, \qquad (16)$$

where α_i is the angle under which the i^{th} triangle is incident to the vertex $v1$ and is computed as the angle between the two edges of the i^{th} triangle incident in the vertex.

PROBLEM DEFINITION

Fig. 7 shows the configuration of open channel flow with a moving free surface. The mean depth of the free surface flow is δ in the normal direction (z). The streamwise direction x along

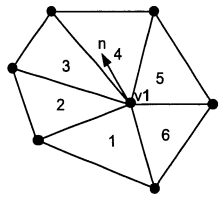

Figure 6: Estimation of the normal direction of a vertex

the channel bed is inclined by angle θ from the horizontal direction. The computational domain size is $2\pi\delta\times\pi\delta\times1.5\delta$ along the streamwise, spanwise and normal directions. There are two homogeneous directions in the streamwise and spanwise directions. The Reynolds number based on the shear velocity at the bed is $\mathrm{Re}_\tau = \frac{u_\tau\delta}{\nu} = 180$. The Froude number based on the bulk mean velocity is $Fr = \frac{U_m}{\sqrt{g\delta}} = 0.6$. This channel flow is gravitationally driven; therefore, the gravitational acceleration along the streamwise direction should balance the gradient of the shear stress on the bed along the normal direction, i.e.,

$$g\sin\theta = \frac{\partial u_\tau^2}{\partial z} = \frac{u_\tau^2|_{z=0}}{\delta}. \qquad (17)$$

If we assume the bulk mean velocity $U_m = 1$, and the mean flow depth $\delta = 1$, the gravitational acceleration component in the streamwise direction is equal to 0.0042318.

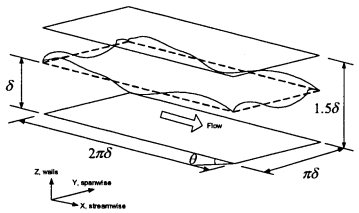

Figure 7: Configuration of open channel flow with moving free surface

The periodic conditions are applied to the two homogenous directions. The non-slip boundary conditions are used on the two walls along the normal direction although the upper wall does not participate in the solution domain in the present one-fluid approach.The computational grids of $64\times64\times192$ nodes are discretized with uniform grid spacings in the streamwise, spanwise and normal direction, respectively.

NUMERICAL RESULTS

Turbulence intensities

The turbulence intensities, $(\overline{u_i'u_i'})^{1/2}$, normalized by the wall shear velocity u_τ, are shown in Fig. 8 together with the LDV experimental results by Komori et al. (1982). The present results are in good agreement with the experimental results. The difference of v' between the predictions and the measurements may be due to the measurement error. As the authors (Komori et al. (1982)) mentioned, it is very difficult to measure v with good accuracy using two-dimensional LDV with the scattering mode.

Near the free surface, the intensity of the streamwise and spanwise fluctuations is increased, and vertical fluctuation is

decreased sharply. This indicates that the turbulent kinetic energy from the vertical component is transferred to the horizontal components near the free surface. This is because the constrained vertical motion is changed to parallel motion, and these motions contribute to the corresponding root-mean-square (RMS) intensities.

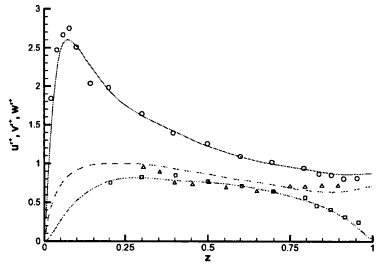

Figure 8: Vertical distributions of turbulence intensities with the comparison of LDV experimental results by Komori et al. (1982). present results: —, u'^+, – – –, v'^+, – · –, w'^+; LDV experimental results: ○, u'^+, △, v'^+, □, w'^+.

Turbulent energy budget

In order to further understand the turbulent behavior near the free surface, we need to investigate the turbulent energy budget for individual velocity correlations. For an incompressible flow, the governing equation for Reynolds stresses can be written as

$$\frac{D\overline{u_i'u_j'}}{Dt} = \underbrace{-\frac{\partial}{\partial x_k}\left(\overline{u_i'u_j'u_k'}\right)}_{\text{Turbulent diffusion}} \underbrace{-\left(\frac{\partial \overline{u_j'p'}}{\partial x_i}+\frac{\partial \overline{u_i'p'}}{\partial x_j}\right)}_{\text{Pressure diffusion}} \underbrace{+\frac{\partial}{\partial x_k}\left(\nu\frac{\partial \overline{u_i'u_j'}}{\partial x_k}\right)}_{\text{Viscous diffusion}}$$
$$\underbrace{-\left(\overline{u_i'u_k'}\frac{\partial \overline{u_j}}{\partial x_k}+\overline{u_j'u_k'}\frac{\partial \overline{u_i}}{\partial x_k}\right)}_{\text{Turbulent production}} \underbrace{-2\nu\overline{\frac{\partial u_i'}{\partial x_k}\frac{\partial u_j'}{\partial x_k}}}_{\text{Dissipation}}$$
$$\underbrace{+\overline{p'\left(\frac{\partial u_i'}{\partial x_j}+\frac{\partial u_j'}{\partial x_i}\right)}}_{\text{Pressure strain}}, \qquad (18)$$

Near the free surface region, Fig. 9 shows the terms for the $\overline{u'u'}$ budget. It can be seen that all terms are significant except for the viscous diffusion and the production terms which go to zero near the free surface. It is interesting to note that the pressure strain term changes sign very close to the surface. This term contributes to the increase of the streamwise component of the turbulent kinetic energy. Fig. 10 shows plots for the $\overline{v'v'}$ budget. It can be seen that the turbulent kinetic energy in the spanwise direction is gained mainly through the pressure strain term, and that there is an increase in the pressure strain after $z^+ > 150$. In Fig. 11, which shows plots for the $\overline{w'w'}$ term, it can be seen that the pressure diffusion term now contributes to the energy budget. All terms have the same relative significance with the pressure strain now being a large energy absorbing term as the free surface is approached.

Fig. 12 shows plots of the three pressure strain terms near the free surface. In this figure, it can be seen clearly that the pressure strain in the $\overline{w'w'}$ equation rapidly decreases in the

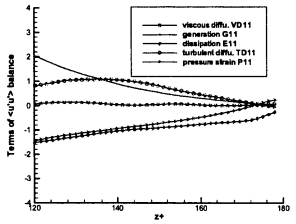

Figure 9: Terms in the budget for $\overline{u'u'}/(u_\tau^3/\delta)$ in wall units.

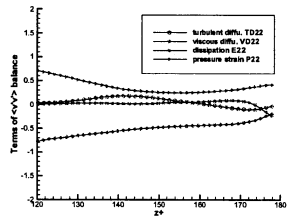

Figure 10: Terms in the budget for $\overline{v'v'}/(u_\tau^3/\delta)$ in wall units.

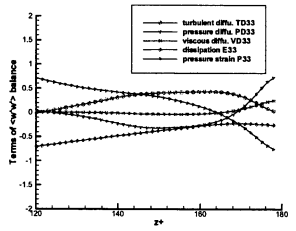

Figure 11: Terms in the budget for $\overline{w'w'}/(u_\tau^3/\delta)$ in wall units.

free surface region and it changes from a positive to a negative value. The pressure strain in the $\overline{v'v'}$ equation is positive and it increases in the surface region. The pressure strain in the $\overline{u'u'}$ equation becomes slightly positive in the vicinity of the free surface. Similar observations have been made by (Komori (1993)). These show that the normal component of the turbulence kinetic energy affected by the free surface is mainly redistributed through the pressure strain terms related to the spanwise motion much more than to the streamwise motion. This confirms that the spanwise turbulence intensity increases more than the streamwise turbulence intensity in the free surface region (see Fig. 8).

Two-point correlation function

The turbulence characteristics near the free surface can be examined by studying a two-point correlation function at different distances below the free surface. The streamwise two-point correlation functions for normal Reynolds stress are defined as:

$$R_{ii}(r_1,z) = \frac{\overline{u_i'(x+r_1,y,z)u_i'(x,y,z)}}{\overline{u_i'(x,y,z)u_i'(x,y,z)}}, \qquad (19)$$

where $i = 1$, 2 or 3 separately, no summation rule. Physically,

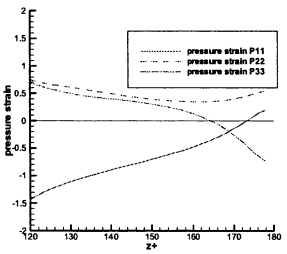

Figure 12: Vertical distribution of the diagonal components of the normalized pressure strain correlation tensor.

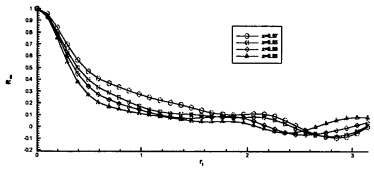

Figure 13: Streamwise two-point correlation function at four vertical locations near the free surface - R_{uu}

if a two-point correlation decays slower, the eddy size in that direction is larger. Figs. 13 to 15 show the streamwise two-point correlation functions at four vertical locations near the free surface.

As can be seen, these two-point correlation profiles show that there is a slower decay of R_{uu} and R_{vv} for increasing r_1 as the free surface is approached. On the other hand, the vertical velocity correlation profile of R_{ww} shows a faster decay with increasing $r_1$as the free surface is approached. This indicates that the eddies in the vertical direction are damped by the free surface and are enlarged in the streamwise direction.

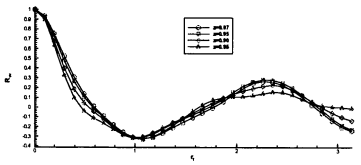

Figure 14: Streamwise two-point correlation function at four vertical locations near the free surface - R_{vv}

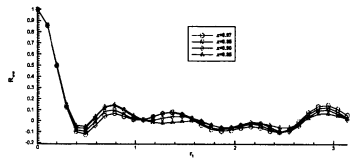

Figure 15: Streamwise two-point correlation function at four vertical locations near the free surface - R_{ww}

CONCLUSIONS

A three dimensional front tracking method is developed and successfully applied to perform LES of free surface flows with small amplitude waves. The triangulated surface meshes with marker points as their vertices are used to represent the free surface and to track its movement. The curved surface is used to compute the volume fraction of fluid, surface area in a Cartesian control domain with Boolean operations. The normal stress boundary conditions are added at the exact location of the free surface. The velocity boundary conditions are computed by the extrapolation method with the least squares technique, which enhances the tangential stress boundary conditions on the interface. From the numerical results of the LES, we can see that the vertical component of the Reynolds stresses is transferred to the horizontal components near the free surface through the pressure strain term. In addition, the normal component of the Reynolds stresses is redistributed to the spanwise motion much more than to the streamwise motion.

REFERENCES

Aftosmis, M. J., Berger, M. J. and Melton, J. E., 1997, "Robust and efficient cartesian mesh generation for component based geometry", Tech. Report AIAA-97-0196, U.S. Air Force Wright Laboratory.

Edelsbrunner, H. and Mucke, E. P., 1990, "Simulation of simplicity: A technique to cope with degenerate cases in geometric algorithms", **ACM Trans. Graph.**, Vol. 9, pp.66-104.

Komori, S., Ueda, H., Ogino, F. and Mizushina, T., 1982, "Turbulence structure and transport mechanism at the free surface in an open channel flow", **International Journal of Heat Mass Transfer**, Vol. 25, pp. 513-521.

Komori, S., Nagaosa, R. and Murakami, Y., 1993, "Direct numerical simulation of three dimensional open channel flow with zero shear gas-liquid interface", **Physics of Fluids**, Vol. 5, pp. 115-124.

Kumar, S., Gupta, R. and Banerjee, S., 1998, "An experimental investigation of the characteristics of free surface turbulence in channel flow", **Physics of Fluids**, Vol. 10, pp. 437-456.

Lilly, D., 1992, "A proposed modification of the Germano subgrid scale closure method", **Physics of Fluids A**, Vol. 3, pp. 32-35.

Nakayama, A. and Yokojima, S., 2002, "Direct numerical simulation of open-channel flow with free-surface fluctuations", **J. Hydraulic, Coastal and Environmental Eng.**, JSCE, No.712/II-60: pp.57-72.

Nezu, I. and Nakagawa, H., 1993, "Turbulence in open channel flows", IAHR Monograph, Balkema publisher, Rotterdam.

Pan, Y. and Banerjee, S., 1995, "A numerical study of free surface turbulence in channel flow", **Physics of Fluids**, Vol. 7, pp. 1649-1663.

Schewchuk, J. R., 1996, "Adaptive precision floating point arithmetic and fast robust geometric predicates", Tech. Report, School of Computer Science, Carnegie Mellon University, Pittsburgh, Pennsylvania.

Thurmer, G. and Wuthrich, C. A., 1998, "Computing vertex normals from polygonal facets", **Journal of Graphics Tools**, Vol. 3, 43-46.

Tryggvason, G. et al., 2001, "A front tracking method for the computations of multiphase flow". **Journal of Computational Physics**, Vol. 169, pp. 708-759.